Particle Filter Based Active Localization of Target and Needle in Robotic Image-Guided Intervention Systems

Mark Renfrew, Zhuofu Bai, M. Cenk Çavuşoğlu
Dept. of Electrical Engineering and Computer Science, Case Western Reserve University, Cleveland, OH 44106
Email: {mxr90,zxb31,cavusoglu}@case.edu

***Abstract*—This paper presents a probabilistic method for active localization of needle and targets in robotic image guided interventions. Specifically, an active localization scenario where the system directly controls the imaging system to actively localize the needle and target locations using intra-operative medical imaging (e.g., computerized tomography and ultrasound imaging) is explored. In the proposed method, the active localization problem is posed as an information maximization problem, where the beliefs for the needle and target states are represented and estimated using particle filters. The proposed method is also validated using a simulation study.**

I. Introduction

Physicians commonly perform needle insertion procedures for diagnostic or therapeutic purposes, such as tissue biopsy or drug delivery. In these procedures, the needle must be inserted in such a way that the needletip intersects a target of interest; a tumor, for example. These procedures are complicated by the fact that needles are subject to bending while inside the tissue, and that the target may move, due either to physiological motions, such as breathing, or due to tissue deformations resulting from the needle-tissue interaction. To mitigate problems caused by the the uncertainty of the target position and the needle configuration, intra-operative medical imaging techniques, such as X-ray fluoroscopy, ultrasound, computerized tomography, and magnetic resonance imaging, can be used to provide real-time information about the needle and target locations, and thus allow the needle to be steered and enabling a closed-loop needle insertion.

In this paper, a probabilistic formulation of the problem of needle and target localization using intra-operative medical imaging is presented. The proposed framework aims to simultaneously localize a target embedded in tissue and a flexible needle as it travels toward a target, the motion of which is modeled stochastically. The probabilistic measurement models account for noise and false detections in the intraoperative medical images. Particle filters are used to track the motions of the needle and target, using the data obtained from the intra-operative imaging systems. An entropy minimization technique is then introduced to actively control the intra-operative imaging system. The proposed models and algorithms are evaluated in simulations using artificial motion and imaging data.

The remainder of this paper is organized as follows. The related work in the literature is briefly described in section II. The models for the target and needle motion and the intra-operative medical imaging, are introduced in section III. The proposed localization and active imaging algorithms are presented in section IV. Simulation results are presented in section V, followed by discussion and conclusions in section VI.

II. Related Work

DiMaio *et al.* [2] first proposed steering flexible needles to reach targets embedded in soft tissue, without touching obstacles or critical areas inside the tissue. DiMaio and Salcudean observed deformations that happen during needle insertion into a gel and simulated needle insertions using a quasi-static finite element method with measured tissue phantom parameters [3]. DiMaio and Salcudean [4] formulated a needle manipulation Jacobian using numerical needle deflection and soft tissue deformation models. In both simulation and experiments, they were able to steer needles to the target in the presence of obstacles in soft tissue by manipulating the needle base.

Webster *et al.* [7], proposed a kinematic model that describe the trajectory of flexible bevel-tip needles in rigid tissue. Parameters were fit using experimental data. Their model did not consider the interaction of the needle with an elastic medium. Misra et al. [9] presented a two dimensional model for a bevel tip needle embedded in an elastic medium. Their mechanics based model is based on both microscopic and macroscopic observations of the needle interaction with soft gels.

Park *et al.* [12] demonstrated a nonholonomic kinematic model to describe how an ideal needle with bevel tip moves through firm tissue with a numerical example. The reachability criteria are proven for this model, and an inverse kinematics method based on the propagation of needle-tip pose probabilities is presented.

Glozman and Shoham [6] developed a needle-steering system with fluoroscopic imaging-based guidance. The system can insert flexible needles with a custom RSPR 6-DOF robot designed to drive the needle tip in a predetermined, curved trajectory by maneuvering the needle base, based on a needle-tissue interaction model. The system can detect the needle tip position and considering natural obstacles, can updated the needle path in real-time. An inverse kinematics algorithm based on a virtual spring model is applied to calculate flexible needle model. More recently, Neubach and Shoham used the same model for flexible needle steering inside soft tissues under real-time ultrasound imaging [10].

Dong *et al.* [5] proposed a framework for localizing needles in ultrasound image frames, in which they formulated the localization problem as a segmentation problem. Their proposed method can track needles in highly noisy ultrasound images during image-guided interventions using level set and partial differential equation based methods.

III. Probabilistic Motion and Measurement Models

This section describes the probabilistic motion and measurement models used as part of the proposed active localization algorithms. Specifically, the needle and target motion models and the models of the intra-operative imaging of the needle and the target will be presented.

A. Motion Models

1) Needle Motion Model: The needle is assumed to be flexible and inserted into a relatively stiff medium. Therefore, the needle will deform while it is being inserted. In this study, a kinematic model is used for the needle. The shape of the needle as it is subjected to deformations is modeled as a piecewise cubic spline. At time t, the shape of the needle is given by the parametric equation

$$\gamma(\lambda)_{j,t} = \mathbf{a}_{j,t} + \mathbf{b}_{j,t}\lambda + \mathbf{c}_{j,t}\lambda^2 + \mathbf{d}_{j,t}\lambda^3, \quad (1)$$

$$j = 1..K,\ 0 \leq \lambda \leq 1, \quad (2)$$

where $\mathbf{a}_{j,t}, \mathbf{b}_{j,t}, \mathbf{c}_{j,t}, \mathbf{d}_{j,t} \in \mathbf{R}^3$ are the coefficients of the spline segment j at time t, K is the number of segments, and λ is the parameter of the splines. The continuity of the needle curve and its tangent direction is enforced by the boundary conditions

$$\gamma(1)_{j,t} = \gamma(0)_{j+1,t} \quad (3)$$

$$\frac{\gamma'(1)_{j,t}}{||\gamma'(1)_{j,t}||} = \frac{\gamma'(0)_{j+1,t}}{||\gamma'(0)_{j+1,t}||} \quad (4)$$

for $j = 1..(K-1)$. The state of the needle at time t, denoted by $x_{\mathrm{n},t}$, can then be defined by the x, y, z coordinates and tangents at the end points of the spline segments, subject to the continuity conditions of (3-4).

The needle control input, $u_{\mathrm{n},t}$, consists of the displacement of the entry point, the change in the tangent direction at the entry point, and the insertion length. In this study, the incremental motion of the needle as it is inserted into the tissue is modeled as a random process to account for uncertainties in the needle motion and deflection. As the proposed active localization algorithms (section IV are based on Bayes' filtering using particle filters, it is sufficient to sample from the motion model $p(x_{\mathrm{n},t}|u_{\mathrm{n},t}, x_{\mathrm{n},t-1})$, instead of computing the posterior probability density function for arbitrary states and inputs.

Given the needle control input, the motion of needle is modeled as the composition of three motion phases. The first phase is the change in the needle configuration as a result of the motion of the needle base, i.e., the displacement of the entry point and the change of the tangent direction. The second phase is the axial insertion of the needle into the tissue. The third phase is the random perturbations to the shape of the needle due to unmodeled tissue-needle interaction forces, which modifies the state of the needle by perturbing the positions and tangents of the control points.

Algorithm 1 is used to generate random samples from $p(x_{\mathrm{n},t}|u_{\mathrm{n},t}, x_{\mathrm{n},t-1})$, for a given prior state $x_{\mathrm{n},t-1}$ and needle control input $u_{\mathrm{n},t}$. Lines 1–4 perturb the commanded control parameters. Line 5 calculates the needle configuration as a result of the base motion. Line 6 then calculates the needle configuration after needle insertion. The final needle configuration is then additionally perturbed by randomly perturbing the positions and tangents of the control points in line 7. Examples of needle insertion simulations are shown in Fig. 1.

2) Target Motion Model: The target is assumed to be a spherical object, with radius R, undergoing Brownian random motion to account for the displacements of the target as a result of unmodeled tissue deformations. The state of the target at time t consists of the x, y, z coordinates of the center of the target, and will be denoted as $x_{\mathrm{g},t}$. Then, each coordinate of the state of the target at time $t + \Delta_t$ will be drawn from a Gaussian

Algorithm 1 Algorithm for generating random samples of needle state, $x_{\mathrm{n},t}$, from prior needle state $x_{\mathrm{n},t-1}$ and needle control input $u_{\mathrm{n},t}$. $u_{\mathrm{n},t}$ consists of the displacement of entry port, d_{b}, rotation of the tangent direction, $\hat{R}_{\mathrm{b}}$, insertion length, l_{i}, and rotation of the needle tip insertion direction, $\hat{R}_{\mathrm{tip}}$. The calculation of the perturbation terms $d_{\mathrm{p}}, R_{\mathrm{p1}}, l_{\mathrm{p}}, R_{\mathrm{p2}}$ have not been included because of space constraints.

function NEEDLEMOTIONSAMPLE(d_{b}, R_{b}, l_{i}, R_{tip})
  $\hat{d}_{\mathrm{b}} \leftarrow d_{\mathrm{b}} + d_{\mathrm{p}}$
  $\hat{R}_{\mathrm{b}} \leftarrow R_{\mathrm{p1}} * R_{\mathrm{b}}$
  $\hat{l}_{\mathrm{i}} \leftarrow l_{\mathrm{i}} + l_{\mathrm{p}}$
  $\hat{R}_{\mathrm{tip}} \leftarrow R_{\mathrm{p2}} * R_{\mathrm{tip}}$
  $x_1 \leftarrow$ NeedleBaseMotion($x_{\mathrm{n},t-1}, \hat{d}_{\mathrm{b}}, \hat{R}_{\mathrm{b}}$)
  $x_2 \leftarrow$ NeedleInsertion($x_1, \hat{l}_{\mathrm{i}}, \hat{R}_{\mathrm{tip}}$)
  $x_{\mathrm{n},t} \leftarrow$ RandomPerturbation(x_2)
return $x_{\mathrm{n},t}$
end function

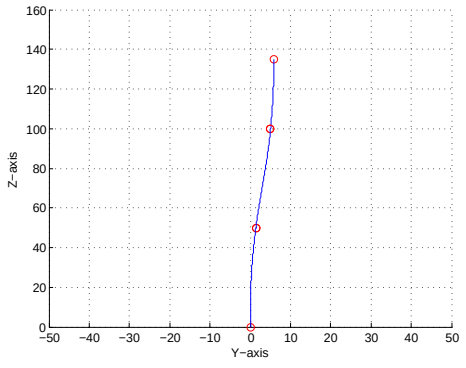

(a)

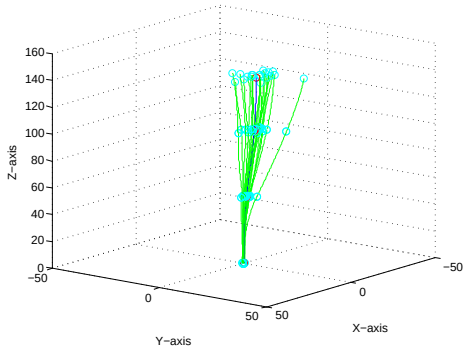

(b)

Fig. 1. (a) An example 4 control point needle, showing flexion of the needle as it is partially inserted into the simulated tissue. (b) 20 samples from the posterior distribution of the needle shape after execution of the needle command shown in (a).

probability density function

$$p(x_{\mathrm{g},t+\Delta_t}|x_{\mathrm{g},t}) = \mathcal{N}(x_{\mathrm{g},t+\Delta_t}; x_{\mathrm{g},t}, \kappa\Delta_t) \qquad (5)$$

where κ is the variance of the Brownian motion for unit time, and $\mathcal{N}(\cdot;\mu,\sigma^2)$ is the normal distribution function with mean μ and variance σ^2. For brevity, in the rest of the paper, the time step Δ_t is not explicitly specified, and, instead, the time variable t is used as integer time index.

B. Measurement Models for the Intra-Operative Medical Imaging System

In many medical imaging technologies, such as ultrasound and computed tomography, the images are acquired serially, and each image represents a single slice of the patient. These images are typically processed using an image processing algorithm, which is used to detect if the target or the needle is present in the image, and, if present, determine their locations. As with any sensor system, measurement of target and needle locations using the intra-operative medical imaging system is prone to measurement errors due to noise. The proposed measurement models explicitly model the inherent uncertainty in the sensor measurements, characterized in the form of a conditional probability distribution function $p(z_t|x_t)$. Here, x_t is the system state, including the needle and target locations as well as the current image plane, and z_t is the measurement vector.

In this study, the image processing performed on the intra-operative medical images is treated as a black-box system, whose output is two logical variables, $z_{\mathrm{nd},t}$ and $z_{\mathrm{td},t}$, which indicate, respectively, if the needle and target have been detected in the current image, and two corresponding image coordinate variables, $z_{\mathrm{nc},t}$ and $z_{\mathrm{tc},t}$, which return the locations of the detected needle and target on the image plane. Furthermore, the measurements of the needle and the target are assumed to be independent, i.e., $p(z_t|x_t) = p(z_{\mathrm{n},t}|x_t)p(z_{\mathrm{g},t}|x_t)$. For notational simplicity, the measurement outputs for detection and location the needle and target are denoted by $z_{\mathrm{n},t}$ and $z_{\mathrm{g},t}$, respectively.

1) Needle Measurement Model: The proposed model of the needle measurement using the intra-operative imaging system incorporates both needle detection errors, i.e., false positives and misses, and error in image locations of correctly detected needle. In a noise free sensor, the needle would be detectable in an image if the needle intersects the current image plane, and the intersection point on the image plane would be the corresponding image coordinates of the detected needle. The visibility of the needle in the "noise-free" image will be denoted by the logical variable I_{n}, where a "true"

value corresponds to an actual intersection between the needle and the image plane, and the corresponding image coordinates will be denoted by $p_{\rm n}$.

In the actual (noisy) imaging system, the needle imaging is assumed to have true positive and false positive rates of $\alpha_{\rm n,tp}$ and $\alpha_{\rm n,fp}$, respectively. Then, the true and false positive probabilities can be written as:

$$p(\mathrm{TP}|x_t) = \begin{cases} \text{if } I_{\rm n} = \text{true}: & \alpha_{\rm n,tp} \\ \text{if } I_{\rm n} = \text{false}: & 0 \end{cases}, \quad (6)$$

$$p(\mathrm{FP}|x_t) = \begin{cases} \text{if } I_{\rm n} = \text{true}: & (1-\alpha_{\rm n,tp})\alpha_{\rm n,fp} \\ \text{if } I_{\rm n} = \text{false}: & \alpha_{\rm n,fp} \end{cases}.$$

Adding the true and false positive rates yield the needle detection probability

$$p(z_{{\rm nd},t} = \text{true}|x_t) = p(\mathrm{TP}|x_t) + p(\mathrm{FP}|x_t)$$
$$= \begin{cases} \text{if } I_{\rm n} = \text{true}: & \alpha_{\rm n,tp} + (1-\alpha_{\rm n,tp})\alpha_{\rm n,fp} \\ \text{if } I_{\rm n} = \text{false}: & \alpha_{\rm n,fp} \end{cases}, \quad (7)$$

and

$$p(z_{{\rm nd},t} = \text{false}|x_t) = 1 - p(z_{{\rm nd},t} = \text{true}|x_t). \quad (8)$$

For a true positive (TP), the measured needle location in the actual (noisy) imaging system is assumed to have zero-mean Gaussian noise. For a false positive (FP), the measured locations is assumed to be uniformly distributed over the image plane. Then, for each of the two coordinates $i = 1, 2$ on the image,

$$p(z^i_{{\rm nc},t}|\mathrm{TP}, x_t) = \mathcal{N}(z^i_{{\rm nc},t}; p^i_{\rm n}, \sigma^2_{{\rm n},i}), \quad (9)$$

$$p(z^i_{{\rm nc},t}|\mathrm{FP}, x_t) = \mathcal{U}(z^i_{{\rm nc},t}; \min_i, \max_i), \quad (10)$$

where $\min_i, \max_i$ is the minimum and maximum coordinates of the image plane in the corresponding dimension, and $\mathcal{U}(\cdot; \min, \max)$ is the uniform distribution function in the domain $[\min, \max]$.

Combining the probability density functions for the needle detection and coordinates, using the conditional probability and total probability equations, yields the probability density function of the needle measurement model as:

$$\begin{aligned} & p(z_{{\rm nd},t}, z^1_{{\rm nc},t}, z^2_{{\rm nc},t}|x_t) \quad (11) \\ = \; & p(z^1_{{\rm nc},t}, z^2_{{\rm nc},t}|z_{{\rm nd},t}, x_t)p(z_{{\rm nd},t}|x_t) \\ = \; & p(z^1_{{\rm nc},t}, z^2_{{\rm nc},t}|\mathrm{TP}, x_t)p(\mathrm{TP}|x_t) \\ & + p(z^1_{{\rm nc},t}, z^2_{{\rm nc},t}|\mathrm{FP}, x_t)p(\mathrm{FP}|x_t) \\ = \; & p(z^1_{{\rm nc},t}|\mathrm{TP}, x_t)p(\mathrm{TP}|x_t)p(z^2_{{\rm nc},t}|\mathrm{TP}, x_t)p(\mathrm{TP}|x_t) \\ & + p(z^1_{{\rm nc},t}|\mathrm{FP}, x_t)p(\mathrm{FP}|x_t)p(z^2_{{\rm nc},t}|\mathrm{FP}, x_t)p(\mathrm{FP}|x_t), \end{aligned}$$

where, in the last step, the independence of the measured needle location's noise in the two dimensions is used. It is important to note that, in the derivations above, the dependence of the needle measurement to the configuration of the imaging plane has not been explicitly included in the equations to simplify the notation.

2) Target Measurement Model: The target measurement model used is very similar to the needle measurement model described above, except for one difference. In the target measurement model, a "true positive" probability value that is a function of the target's cross section area visible in the image plane is used instead of a constant true positive rate. Specifically, the "true positive" detection probability is defined as:

$$p_{\rm tp}(x_t) = \begin{cases} A_{\rm g} \geq A_o & : \quad A/A_o \\ A_{\rm g} \geq A_o & : \quad 1 \end{cases} \quad (12)$$

where $A_{\rm g}$ is the target's cross section area visible in the image plane, and A_o is a critical area above which the detection probability is equal to 1. Then the true and false positive probabilities for target detection can be written as:

$$p(\mathrm{TP}|x_t) = \begin{cases} \text{if } I_{\rm g} = \text{true}: & p_{\rm tp}(x_t) \\ \text{if } I_{\rm g} = \text{false}: & 0 \end{cases}, \quad (13)$$

$$p(\mathrm{FP}|x_t) = \begin{cases} \text{if } I_{\rm n} = \text{true}: & (1-p_{\rm tp}(x_t))\alpha_{\rm g,fp} \\ \text{if } I_{\rm n} = \text{false}: & \alpha_{\rm g,fp} \end{cases},$$

where the variables are defined analogously to the needle model case. The remaining equations of the target measurement model are similar to the needle measurement equations (7-11), with the relevant variables defined in an analogous way, and will not be repeated here. Similar to the needle measurement model equations, the dependence of the target measurement on the configuration of the imaging plane has not been explicitly included in the equations in order to simplify the notation.

IV. Active Localization Algorithms

In this study, a scenario where the system directly controls the imaging system to actively localize the needle and target locations using various forms of intra-operative imaging (e.g., computerized tomography, and ultrasound imaging) is explored. This active localization problem are posed as an information maximization problem (e.g., [1], [14], [8]), where the beliefs for the needle and target states will be represented and estimated using particle filters.

A. Needle and Target Localization

In order to reduce the computational complexity of the problem by reducing the dimensionality of the state, the beliefs of the target and needle states will be estimated by using two separate particle filters; one to track the target, and the other to track the needle. Algorithm 2 shows the particle filtering algorithm used for needle

localization (adapted from the generic particle filter algorithm, e.g., from [14]). The algorithm for the target localization is analogous.

The particle filter for localizing the needle uses particles of dimension $6K$, where K is the number of control points. These dimensions correspond to the position and tangent vectors for each control point, and each particle represents a possible needle shape. The particle filter for localizing the target uses 3-dimensional particles that represent possible (x, y, z) positions of the target.

Algorithm 2 Particle filtering algorithm for needle localization. $\mathcal{B}_{\mathrm{n},t} = \{x_{\mathrm{n},t}^{[n]},\ n = 1..N\}$ is the set of particles that represent the belief of the needle state at time t. N is the number of particles used.

function UPDATENEEDLEBELIEF($\mathcal{B}_{\mathrm{n},t-1}$, $u_{\mathrm{n},t}$, $z_{\mathrm{n},t}$)
  $\bar{\mathcal{B}}_{\mathrm{n},t} \leftarrow \emptyset$
  $\mathcal{B}_{\mathrm{n},t} \leftarrow \emptyset$
  for $n = 1 \rightarrow N$ **do**
    sample $x_{\mathrm{n},t}^{[n]} \sim p(x_{\mathrm{n},t}|u_{\mathrm{n},t}, x_{\mathrm{n},t-1}^{[n]})$
    $w_t^{[n]} \leftarrow p(z_{\mathrm{n},t}|x_t^{[n]})$
    $\bar{\mathcal{B}}_{\mathrm{n},t} \leftarrow \bar{\mathcal{B}}_{\mathrm{n},t} + (x_{\mathrm{n},t}^{[n]}, w_t^{[n]})$
  end for
  $\mathcal{B}_{\mathrm{n},t} \leftarrow$ LowVarianceSampler($\bar{\mathcal{B}}_{\mathrm{n},t}$)
return $\mathcal{B}_{\mathrm{n},t}$
end function

B. Active Localization Using Information Maximization

In active localization, the system actively controls one or more of the control inputs to maximize information about the state of the system. In the considered application there is a natural decomposition of the control inputs of the system. The intra-operative medical imaging system can be controlled to actively localize the needle and the target, while the needle control inputs can be used to execute the task (such as, direct the needle towards the target). In this study, a greedy exploration algorithm based on entropy minimization is employed (Algorithm 3). In the algorithm, the entropy of the needle and target's beliefs, which are represented using particle filters, are estimated using the differential entropy calculation approach [11], [13].

V. SIMULATION RESULTS

The proposed models and algorithms are demonstrated by the following simulated needle insertion task and observing the performance of the algorithms in tracking the needle and the target.

In the simulation experiment, a computerized tomography (CT) system is used as the intra-operative imaging system. The slices of the CT scanner are orthogonal to the initial needle insertion direction. The scanner has needle and target measurement error variances of $\sigma_{\mathrm{n},i}^2 = \sigma_{\mathrm{g},i}^2 = (0.2\ \mathrm{mm})^2$, with $\alpha_{\mathrm{n,fp}} = 0.02$, $\alpha_{\mathrm{n,tp}} = 0.98$, $\alpha_{\mathrm{g,fp}} = 0.01$, and $A_o = 75\ \mathrm{mm}^2$. In order to reduce the computational complexity, at the expense of reduced resolution, CT scanner image planes are assumed to be positioned in 5 mm increments. The needle is aimed at a 0.5 mm radius target at depth of approximately 140 mm from the needle entry point. The location of the target is not initially known by the system, except for the fact that it lies in a $(60\ \mathrm{mm})^3$ region. The target is also undergoes Brownian motion with $\kappa\Delta t = (0.1\ \mathrm{mm})^2$.

The target region is initially scanned linearly in 12 steps to locate the target. In the initial scanning phase, only the target localization algorithm is executed, as the needle is not inserted, and the imaging is performed linearly. Once the target is located, the needle is inserted straight towards the target in 27 steps, each with 5 mm insertion increments. Although the model used in

Algorithm 3 Greedy active localization algorithm based on entropy minimization. Here, it is assumed that the needle control input u_{n} is separately determined by a needle motion planner and controller based on the current beliefs of needle and target states. Also, the dependence of the needle and target measurements to the configuration of the image plane, specified by u_{i}, is explicitly included in the measurement model expressions for clarity.

function ACTIVELOCALIZATION($\mathcal{B}_{\mathrm{n},t}$, $\mathcal{B}_{\mathrm{g},t}$, $u_{\mathrm{n},t+1}$)
  $\rho_u \leftarrow 0$ for all image plane configurations u_{i}
  for $n = 1 \rightarrow N_{\mathrm{n}}$ **do**
    for all image plane configurations u_{i} **do**
      sample $x'_{\mathrm{n}} \sim p(x'_{\mathrm{n}}|u_{\mathrm{n},t+1}, x_{\mathrm{n},t}^{[n]})$
      sample $z'_{\mathrm{n}} \sim p(z'_{\mathrm{n}}|x'_{\mathrm{n}}, u_{\mathrm{i}})$
      $\mathcal{B}'_{\mathrm{n}} \leftarrow$ UpdateNeedleBlf($\mathcal{B}_{\mathrm{n},t}$, $u_{\mathrm{n},t+1}$, z'_{n})
      $\rho_u \leftarrow \rho_u -$ Entropy($\mathcal{B}'_{\mathrm{n}}$)
    end for
  end for
  for $n = 1 \rightarrow N_{\mathrm{g}}$ **do**
    for all all image plane configurations u_{i} **do**
      sample $x'_{\mathrm{g}} \sim p(x'_{\mathrm{g}}|x_{\mathrm{g},t}^{[n]})$
      sample $z'_{\mathrm{g}} \sim p(z'_{\mathrm{g}}|x'_{\mathrm{g}}, u_{\mathrm{i}'})$
      $\mathcal{B}'_{\mathrm{g}} \leftarrow$ UpdateTargetBelief($\mathcal{B}_{\mathrm{g},t}$, z'_{g})
      $\rho_u \leftarrow \rho_u -$ Entropy($\mathcal{B}'_{\mathrm{g}}$)
    end for
  end for
return $\arg\max_u \rho_u$
end function

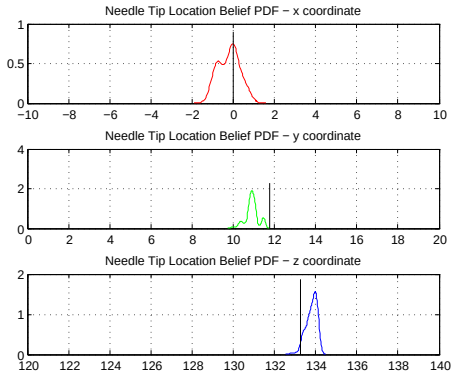

(a)

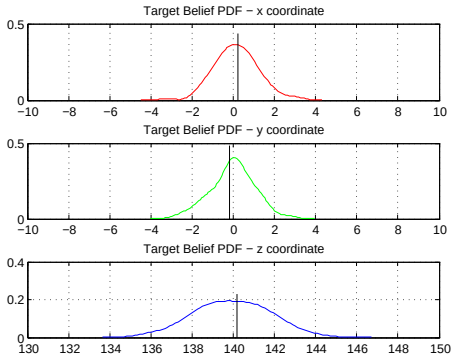

(b)

Fig. 2. Kernel smoothed density estimates for the needle tip (a) and target (b) location beliefs. The solid vertical lines indicate the actual value of the needle tip / target location.

the active localization algorithm assumes a nominally straight needle, the actual needle used has a bevel tip. The bevel tip of the needle would result in a lateral deviation of approximately 12 mm in the actual needle trajectory, for the 140 mm needle insertion (effective curvature of 1.410^{-3} mm^{-1}). For illustration purposes, the needle is inserted in open loop mode, without any explicit feedback control, in order to investigate if the needle will be successfully localized or not.

The performance of the proposed algorithm was measured by performing 20 repetitions of this experiment and measuring the error between the actual and estimated (using expected value of the belief functions) locations of the needle tip and target. The resulting absolute needle tip and target localization errors were 0.80 ± 0.36 mm, and 0.68 ± 0.35 mm (mean $\pm$ standard deviation), respectively.

Fig. 2, 3, and 4 shows sample results from the simulated needle insertion tasks. Fig. 4 shows the active localization algorithm's beliefs of the needle and target at four different steps in a sample execution of the task.

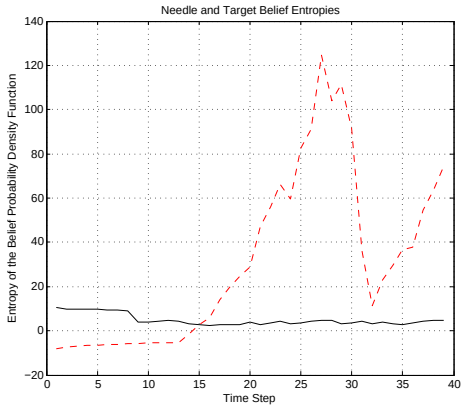

Fig. 3. Change in the entropies of the needle tip (dashed) and target (solid) location beliefs during a sample execution of the task. As it can be seen from the figure, the algorithm successfully alternates between imaging the target and the needle in order to minimize the total entropy of the belief.

As it can be seen from the figure, the active localization algorithm was successfully able to accurately capture the deviated shape of the needle. Fig. 2 shows the kernel smoothed density estimates for the target and needle tip location beliefs, estimated from the corresponding particle filter outputs, at the end of a sample execution of the task. The results indicate that the target and needle locations were estimated accurately. Finally, Fig. 3 shows the change in the entropies of the target and needle tip location beliefs during a sample execution of the task. As it can be seen from the figure, the algorithm successfully alternates between imaging the target and the needle in order to minimize the total entropy of the belief.

VI. Discussion and Conclusions

This paper describes the formulation of a framework for active localization of a flexible needle and targets embedded in the tissue in needle-based image-guided medical interventions. In this proposed paradigm, the system directly controls the imaging system, as the needle is being inserted into tissue, to actively localize the needle and target locations using intra-operative medical imaging data (e.g., from computerized tomography, or ultrasound imaging). The uncertainties in the needle and target motions as well as the imaging system have been explicitly considered using a probabilistic formulation. The proposed algorithms were successfully validated using a simulation study.

The simulation results indicated that the proposed algorithms were able to localize the needle and the target with accuracy comparable to the imaging resolution. Furthermore, the proposed active localization approach, which greedily minimized the entropy of the target and

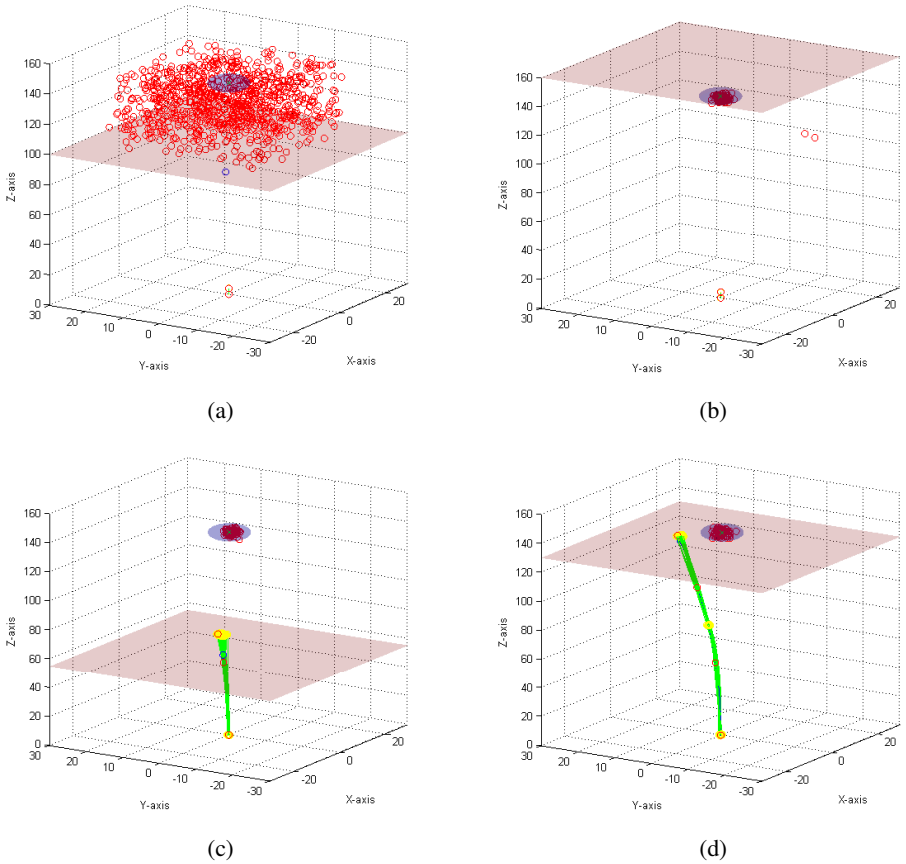

Fig. 4. The particle filter tracking the needle and target. The blue line (invisible) is the actual needle shape, the green lines are the shapes of the particles in the needle belief function, the large semi-transparent sphere is the actual target, the red circles are the centers of the particle in the target belief function, and the semi-transparent plane is the current imaging plane. (a) Initial particle distribution when the location of the target is unknown. (b) The target is localized at the end of the linear scanning phase. (c) Particle distribution at the mid point of the needle insertion. (d) Particle distribution at the end of the task. Figures show that the algorithm successfully localizes the needle and target configurations.

needle state belief probability density functions, was successful in simultaneously localizing the target and the needle by alternating between imaging the target and the needle as necessary.

It is important to note that the presented results, which only includes a simulation based validation study, is intended as a proof-of-concept of the proposed active localization approach for robotic image-guided interventions under intra-operative imaging assistance. A hardware validation of the proposed algorithms using data from an actual intra-operative medical imaging system is a subject of future work.

Computation time, which has not been addressed in the current study, is an important concern as it is in any particle filter-based algorithm for high dimensional state spaces. In the current implementation with MATLAB (version 7.11), one time step of the algorithm, which includes execution of needle and target state belief updates (Algorithm 2) and the entropy minimization computation (Algorithm 3), takes 88 seconds on a PC with 2.66 GHz Intel Xeon processor and 8 GB of memory. A real-time implementation of the proposed algorithm is a subject of the future work. The necessary speedup can potentially be achieved by a more computationally efficient implementation, and by employing parallel processing (including, GPU-based computation), as particle filtering algorithms can be trivially parallelized.

ACKNOWLEDGMENTS

This work was supported in part by the National Science Foundation under grants IIS-0805495, IIS-0905344, and CNS-1035602, and the National Institutes of Health under grant R21 HL096941.

REFERENCES

[1] H. Choset, K. M. Lynch, S. Hutchinson, G. Kantor, W. Burgard, L E. Kavraki, and S. Thrun. *Principles of Robot Motion: Theory, Algorithms, and Implementations,*. MIT Press, 2005.

[2] S. P. DiMaio. *Modelling, simulation and planning of needle motion in soft tissue*. Ph.d., University of British Columbia, Vancouver, Canada, 2003.

[3] S.P. DiMaio and S.E. Salcudean. Needle insertion modeling and simulation. *Robotics and Automation, IEEE Transactions on*, 19(5):864 – 875, 2003.

[4] S.P. DiMaio and S.E. Salcudean. Needle steering and motion planning in soft tissues. *Biomedical Engineering, IEEE Transactions on*, 52(6):965 –974, 2005.

[5] B. Dong, E. Savitsky, and S. Osher. A novel method for enhanced needle localization using ultrasound-guidance. In *Advances in Visual Computing*, volume 5875 of *Lecture Notes in Computer Science*, pages 914–923. Springer Berlin / Heidelberg, 2009.

[6] D. Glozman and M. Shoham. Image-guided robotic flexible needle steering. *Robotics, IEEE Transactions on*, 23(3):459 – 467, 2007.

[7] R. J. Webster III, J. S. Kim, N. J. Cowan, G. S. Chirikjian, and A. M. Okamura. Nonholonomic modeling of needle steering. *International Journal of Robotics Research*, 25(5-6):509–525, May-June 2006.

[8] S. M. LaValle. *Planning Algorithms*. Cambridge University Press, 2006.

[9] S. Misra, K.B. Reed, B.W. Schafer, K.T. Ramesh, and A.M. Okamura. Observations and models for needle-tissue interactions. In *Robotics and Automation, 2009. ICRA '09. IEEE International Conference on*, pages 2687–2692, May 2009.

[10] Z. Neubach and M. Shoham. Ultrasound-guided robot for flexible needle steering. *Biomedical Engineering, IEEE Transactions on*, 57(4):799–805, 2010.

[11] U. Orguner. Notes on differential entropy calculation using particles. Technical report, Department of Electrical Engineering, Linkping University, 2008.

[12] W. Park, J. S. Kim, Y. Zhou, N.J. Cowan, A.M. Okamura, and G.S. Chirikjian. Diffusion-based motion planning for a nonholonomic flexible needle model. In *Proc. of the IEEE In'l Conf. on Robotics and Automation*, pages 4600–4605, 2005.

[13] A. Ryan and J. K. Hedrick. Particle filter based information-theoretic active sensing. *Robotics and Autonomous Systems*, 58(5):574–584, 2010.

[14] S. Thrun, W. Burgard, and D. Fox. *Probabilistic Robotics*. MIT Press, 2005.